ACS APPLIED MATERIALS & INTERFACES

Research Article

www.acsami.org

Boron-Doped Silicon Diatom Frustules as a Photocathode for Water Splitting

Soundarrajan Chandrasekaran,[†] Thomas J. Macdonald,[‡] Andrea R. Gerson,[†,§] Thomas Nann,*[,‡] and Nicolas H. Voelcker*[,†]

[†]Mawson Institute, [‡]Ian Wark Research Institute, [§]Minerals and Materials Science & Technology, University of South Australia, Mawson Lakes Boulevard, Adelaide, SA 5095, Australia

Supporting Information

ABSTRACT: An effective solar-powered silicon device for hydrogen production from water splitting is a priority in light of diminishing fossil fuel vectors. There is increasing demand for nanostructuring in silicon to improve its antireflective properties for efficient solar energy conversion. Diatom frustules are naturally occurring biosilica nanostructures formed by biomineralizing microalgae. Here, we demonstrate magnesiothermic conversion of boron-doped silica diatom frustules from *Aulacoseira* sp. into nanostructured silicon with retention of the original shape. Hydrogen production was achieved for boron-doped silicon diatom frustules coated with indium phosphide nanocrystal layers and an iron sulfur carbonyl electrocatalyst.

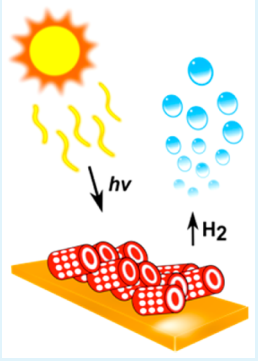

KEYWORDS: *boron, silicon, diatom frustules, photocatalysis, hydrogen*

INTRODUCTION

According to the Smalley Institute, the number one challenge that humanity will face in the coming 50 years is energy. More specifically, the actual challenge lies in the storage and distribution of renewable energy as conversion becomes economically viable. The most versatile method for renewable energy storage is the production of a fuel in which hydrogen (H_2), via water splitting, is an important product or intermediate.[1−4] Solar water splitting involves the photoelectrochemical production of H_2 using n- and p-type semiconductors, which have been used to harvest sunlight to oxidize and reduce water, respectively.[3] Silicon is an ideal semiconductor photoelectrode when compared with a range of prevalent semiconductors because to its abundance and low band gap (1.12 eV).[5,6] In addition to bulk silicon, nanostructured silicon, such as porous silicon and silicon nanowires, has been demonstrated to be suitable for solar energy conversion due to its tunable band gap and antireflective surfaces.[7−9] Recently, enhancements in solar energy conversion have been made possible using nontoxic semiconductor nanocrystals (NC) that act as light antennas to maximize visible light absorption for energy conversion.[10−12] The fabrication of hybrid nanostructured silicon photoelectrodes coated with NCs and an inexpensive bioinspired electrocatalyst is a desirable goal. Indium phosphide nanocrystals (InP NCs) and iron sulfur carbonyl catalyst ($Fe_2S_2(CO)_6$) on silicon have previously been shown to improve the efficiency of solar energy conversion.[9,13] These devices are not only useful for H_2 generation but also for optoelectronic and photovoltaic devices.[14]

Diatoms are photosynthetic microalgae that are commonly found in seawater.[15] In diatoms, nanostructured porous silica is formed as a result of the biomineralization process.[15] The frustule of the diatom *Aulacoseira* sp. has a hollow cylindrical shape that is ∼4−6 μm in diameter and ∼10−20 μm in length. The walls of the diatom frustules contain pores spaced in an orderly fashion with diameters of ∼400−500 nm.[16]

Since diatom frustules are naturally abundant, resulting in low cost and reduced fabrication requirements, they serve as an excellent alternative to silicon nanostructures. Recently, extensive research into the modification of diatom frustules for use in drug delivery and optoelectronic and photovoltaic applications has been carried out.[17−22] Diatom frustules are not suitable for photovoltaic applications without modification since silica is an insulator. The modifications that make them suitable for photovoltaic applications include biological insertion of titania[17] and plasma-polymerized coating of titania.[23]

Recently, these silica diatom frustules have been converted into silicon (solar absorber) while retaining their original shape using a magnesiothermic approach for sensing applications.[24] We demonstrated n-type behavior of these converted silicon

Received: May 28, 2015
Accepted: July 20, 2015
Published: July 20, 2015

DOI: 10.1021/acsami.5b04640
ACS Appl. Mater. Interfaces 2015, 7, 17381−17387

diatom frustules through photocurrent measurements for solar water electrolysis applications.[25]

A chemical procedure involving the doping of silicon nanoparticles using boric acid as a precursor was described by Ge et al.[26] The boron-doped silicon nanoparticles were used as anode materials for battery applications. Herein, we doped silica diatom frustules with boron and then magnesiothermically converted them into p-type silicon diatom frustules. We were able to retain the shape of the diatom frustules after doping and magnesiothermic conversion. The boron-doped silicon diatom frustules were then deposited on a gold-coated glass slide as a photocathode for water electrolysis. After coating the diatom frustules with InP NCs $Fe_2S_2(CO)_6$, the fabricated electrodes were assembled into a three-electrode electrochemical cell for photocurrent measurements, and the H_2 produced in the headspace was analyzed using a gas chromatograph (GC).

EXPERIMENTAL SECTION

Materials. Purified diatom silica frustules were kindly provided by Professor Dusan Losic from University of Adelaide. HF (48%) was purchased from Scharlau Chemie (Chem-Supply Pty. Ltd. Australian representation), and boric acid, from May and Baker, Australia. InP NCs were synthesized by a method described elsewhere.[27,28] All other chemicals were purchased from Sigma-Aldrich (Australia) unless otherwise stated.

Magnesiothermic Conversion of Silica Diatom Frustules to Silicon. A 0.5:1 weight ratio of magnesium turnings to silica diatom frustules was mixed thoroughly in a tungsten boat. Subsequently, the mixture was heated to 650 °C at a ramping rate of 10 °C per min and kept for 7 h in a tube furnace under a flow of argon gas (99.995%). After cooling, the heating procedure was repeated again after thoroughly mixing the products formed to ensure the complete conversion of silica diatom frustules to silicon. The formed products were then washed in HCl and HF solutions to remove magnesium oxide and any oxide layer formed in the silicon surface, respectively, and stored in a glovebox (high-purity argon gas (99.997%)). This procedure was adapted from Chandrasekaran et al.[25]

Boron Doping of Silicon Diatoms Frustules. Boric acid was used as a precursor for boron doping. A weight ratio of 1:1 silicon diatom frustules to boric acid was placed in a silica crucible. This was then mixed with an equal ratio of milli-Q water to wet all surfaces. Subsequently, the mixture was heated in a tube furnace under a flow of argon gas (99.995%) at a ramping rate of 15 °C per min and was kept at 900 °C for 3 h. After cooling, the products were gently stirred in a 5% HF solution and then rinsed in milli-Q water. This doping procedure was adapted from Ge et al.,[26] in which they used silicon nanoparticles as the starting material.

Boron Doping of Silica Diatom Frustules. Boric acid and silica diatom frustules at a 1:1 weight ratio were placed in a silica crucible and then mixed with an equal ratio of milli-Q water to wet all surfaces. In additional experiments, boric acid and silica diatom frustules were mixed at weight ratios of 0.5:1 and 2:1, respectively. This mixture was then heated to 900 °C at a ramping rate of 15 °C per min and kept for 3 h in a tube furnace under a flow of argon gas (99.995%). After cooling, the products were washed with milli-Q water and centrifuged at 14 500 rpm for 2 min; this process was repeated five times.

Magnesiothermic Conversion of Boron-Doped Silica Diatom Frustules. Synthesized boron-doped silica was converted into boron-doped silicon using the shape retention magnesiothermic conversion procedure previously explained.

Inductively Coupled Plasma Mass Spectrometry (ICP-MS) Analysis. The sample solution was prepared by adding 1 mg of the sample to 2 mL of 10 M NaOH followed by sonication at 60 °C for 5 h or until the sample was completely dissolved. The sample solution was then centrifuged at 14 500 rpm for 5 min to confirm sample dissolution. The solution was then adjusted to 20 mL by adding milli-Q water and 10 μL of concentrated nitric acid. The working solution was prepared by adding 1 mL of the sample solution to 9 mL of milli-Q water. An Agilent triple quadrupole ICP-MS (ICP-QQQ 8800, Tokyo, Japan) was used for silicon and boron solution assays. Measurements were carried out in two gas modes (He and O_2). The MS/MS mass-shift mode with O_2 reaction gas (0.40 mL min^{-1}) was used to measure silicon as SiO^+ at 44 m/z (Q1 = 28 and Q2 = 44). Boron was measured in single quadrupole (m/z = 11) using He gas mode (5.0 mL min^{-1}). All acids used were either analytical reagent (AR) or trace analysis grade (TAG) from Fisher Scientific, UK; milli-Q water (≥18.2 MΩ cm) was used throughout. Internal standards included Sc and Ir (100 μg L^{-1}) in 2% v/v TAG HNO_3. Stock single element solutions containing 1000 mg L^{-1} of silicon and boron (high-purity standards, Australia) were used to prepare the external calibration standard solution by diluting them in 2% v/v TAG HNO_3. The same standards were used for preparation of the continuing calibration verification (CCV) standards for quality control purposes (recoveries were 98.4% silicon and 99.5% boron).

Surface Functionalization. Boron-doped silicon diatom frustules were thermally hydrosilylated in a 1 M toluene solution of allyl mercaptan (AM) at 50 °C for 15 h. They were then purified by washing with absolute toluene (three times), vacuum dried, and stored in a glovebox. This procedure was reproduced from Chandrasekaran et al.[25]

InP NCs Synthesis. InP NCs were synthesized using a method adapted from Xu et al.[27,28] Briefly, stearic acid (0.1 mmol), zinc undecylenate (0.2 mmol), indium(III) chloride (0.1 mmol), and hexadecylamine (0.2 mmol) were added to a N_2-purged Schlenk flask. Organic ligand 1-octadecene (~2 mL) was added, and the mixture was vacuum/backfilled with N_2 before heating at 270 °C. Upon reaching 270 °C, a solution of tris(trimethylsilyl)phosphine (1 mL, 0.1 M) in 1-octadecene was rapidly injected, causing the temperature of the solution to drop to 250 °C. Upon injection, the NCs were allowed to grow for 10 min at 250 °C, causing a color change to deep red. The flask was then cooled to room temperature, and the NCs were washed twice with ethanol (2 × 60 mL) to remove any excess ligands and redispersed in toluene (10 mL).

Electrode Fabrication. One-hundred microliters of a 1 mg mL^{-1} toluene solution of AM hydrosilylated boron-doped silicon diatom frustules was drop-casted on a gold-coated glass slide in a glovebox. After drying, this process was repeated five times. The surface was then gently washed with distilled water to remove the unbound boron-doped silicon diatom frustules. The hybrid electrode was fabricated by adding five layers of InP NCs, and the surface was then gently washed with distilled water to remove the unbound InP NCs. Finally, a layer of $Fe_2S_2(CO)_6$ catalyst in toluene was dried onto the surface.

Surface Characterization. Scanning electron microscopy (SEM) images and energy dispersive X-ray absorption spectroscopy (EDXS) spectra were obtained using a FEI Quanta 450 environmental scanning electron microscope (ESEM). X-ray diffraction (XRD) spectra of the samples were recorded on a Scintag X'TRA (ARL Applied Research Laboratories, VA, USA) X-ray diffractometer with the Scintag Peltier cooled Si(Li) solid-state detector. The elemental surface chemical composition was analyzed using a Kratos AXIS Ultra DLD X-ray photoelectron spectrometer (XPS) operating with monochromatic Al Kα radiation at 300 W. Spectrometer pass energies of 160 and 20 eV were employed for survey and high-resolution scans, respectively.

Si K-edge X-ray absorption near edge structure (XANES) spectra were collected on the Soft X-ray Spectroscopy beamline at the Australian Synchrotron (Melbourne, Australia), operating at 3 GeV with a beam current at 200 mA. Six to eight pieces of In foil (3 × 4 mm^2) were attached to the Au plate of the sample holder using double-sided carbon tape. The powder samples were pressed onto these indium foils, transferred, and loaded into the spectrometer under an inert atmosphere. X-ray absorption spectra were recorded in partial electron yield (PEY) detection mode across the photon energy range of 1820−1915 eV with 0.1 eV steps and 0.5 s integration time using a microchannel plate detector. A silicon wafer was used to calibrate the Si K-edge XANES spectra. The Athena software package[29] in conjunction with plotting software (Excel and Origin) was used for data processing, including extraction, normalization, and smoothing.

DOI: 10.1021/acsami.5b04640
ACS Appl. Mater. Interfaces 2015, 7, 17381−17387

Photocurrent and GC Measurements. Irradiation was performed using an Abet solar simulator (air mass 1.5−1 sun) and calibrated against a silicon solar cell (New-Spec). Electrochemical measurements were carried out using a PG 310 potentiostat from HEKA Electronics (Germany). Electrolysis was performed using a sealed three-electrode Teflon photoelectrochemical cell consisting of a Pt counter electrode, a Ag|AgCl 3 M KCl reference electrode, and a working electrode. The working electrode was illuminated with a light intensity of 100 mW cm^{-2} under air mass 1.5 conditions with a short 12 s dark−light cycle to measure the photocurrents as a function of time. The potential between the working and reference electrodes was adjusted between 0 and −500 mV in 100 mV steps. The long run photocurrents were measured under a light cycle at a bias voltage of −500 mV, which depended on the open-circuit potential (OCP). The sample gas in the headspace (310 μL) above the electrolyte was sampled after 1 h and analyzed using a SRI 310C series GC with a thermal conductivity detector and a column held at 70 °C in N_2 as the carrier gas.

RESULTS AND DISCUSSION

XANES Study of Conversion of Silica to Silicon Diatom Frustules. Silicon 1s XANES was used to confirm (Figure 1) complete magnesiothermic conversion of the diatom

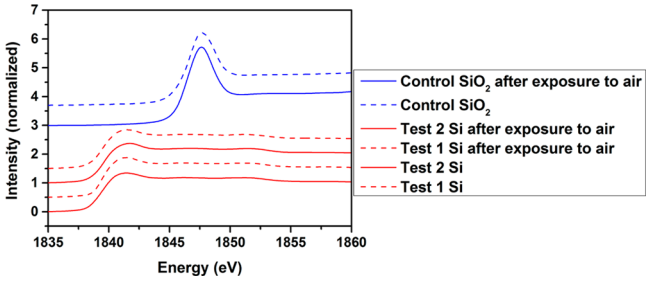

Figure 1. XANES spectra confirm the conversion of silica diatom frustules to elemental silicon. The red traces represent silicon, and the blue traces represent control silica.

frustules from undoped silica to elemental silicon. Edge energies (peak maxima) of approximately 1840 eV indicated the presence of elemental silicon[30] (red spectra), whereas the shape of the top two blue spectra from the nontreated frustules confirmed the presence of amorphous silica.[31]

Boron Doping of Silicon Diatom Frustules. We observed that the shape retention was poor when boron doping was performed using silicon diatom frustules as the starting material at 900 °C in an argon atmosphere. This was attributed to the HF treatment step that was aimed at removing the resulting silicon oxide layer from the frustule surface, as seen in the SEM image shown in Figure S1. For this reason, thermal boron doping at 900 °C was carried out on the silica diatom frustule before performing the magnesiothermic conversion step.

SEM images were used to confirm that the shape of the diatom frustules was retained for boron-doped silica and subsequently upon magnesiothermic conversion to boron-doped silicon (Figure 2, panels A and B, respectively). The attenuation of the oxygen signal in the EDXS spectra confirmed that the magnesiothermic conversion was efficient (Figure 2C,D).

XPS measurements confirmed the presence of boron species in both silica (Figure 3A) and magnesiothermically converted silicon diatom frustules (Figure 3B) after doping. The peak value of 193.2 eV seen for the boron-doped silica diatom frustules corresponds to boron oxide,[32] whereas in boron-

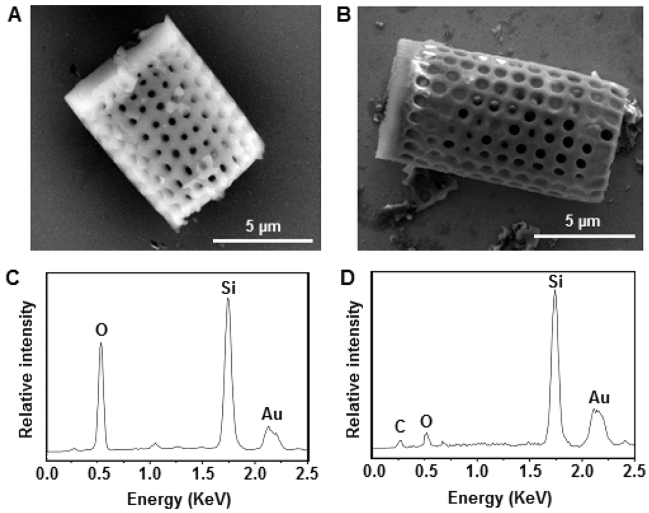

Figure 2. (A, B) SEM images of boron-doped diatom silica and silicon (magnesiothermically converted), respectively. (C, D) EDXS spectra corresponding to A and B, respectively. The attenuation of the oxygen peak (D) confirms the magnesiothermic conversion.

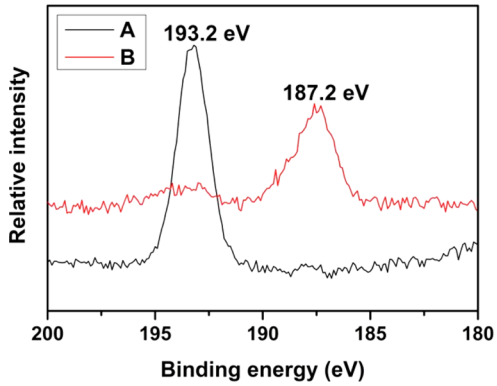

Figure 3. Boron 1s XPS spectra of boron-doped diatom silica and silicon (magnesiothermically converted), traces A and B, respectively. The peak at 187.3 eV confirms the presence of elemental boron in silicon diatom frustules, whereas the peak value at 193.2 eV indicates the presence of boron oxide.

doped silicon diatom frustules, elemental boron (peak value = 187.2 eV)[33] dominated. The survey spectrum also confirms a reduction of the oxygen peak after conversion (Figure S2B) when compared to preconversion peaks (Figure S2A). The residual oxygen content in Figure S2B (after conversion) was attributed to oxides of boron and surface oxidation of silicon diatom frustules.

Figure S3 shows the XRD pattern of boron-doped silicon diatom frustules. There is no appreciable change in the silicon peaks (JCPDS card no. 27-1402) present in the diffraction spectrum of boron-doped silicon frustules compared to the spectrum of undoped silicon diatom frustules previously published.[25] The quantification of elemental boron concentration was carried out using ICP-MS (Table 1). For a 1:1 weight ratio of boric acid to silica diatom frustules, the boron concentration in doped silica diatom frustules was 1.185 ± 0.086 ppm. A 1.25-fold decrease in boron concentration (0.953 ± 0.054 ppm) in silicon diatom frustules, as compared to that in silica diatom frustules, was observed. This may be due to the loss of boron upon washing with hydrochloric acid (HCl) and the HF treatment steps that are required for the removal of

DOI: 10.1021/acsami.5b04640
ACS Appl. Mater. Interfaces 2015, 7, 17381−17387

Table 1. Measured Concentrations of Elemental Boron for Boric Acid (Control) and Different Boron-Doped Samples with Different Boric Acid-to-Silica Weight Ratios (0.5:1, 1:1, and 2:1)

samples	boron concentration (ppm)		
	0.5:1	1:1	2:1
boric acid	4.158 ± 0.126	8.110 ± 0.109	16.879 ± 0.195
boron-doped silica diatom frustules	0.774 ± 0.184	1.185 ± 0.086	2.574 ± 0.123
boron-doped silicon diatom frustules	0.553 ± 0.071	0.953 ± 0.054	1.072 ± 0.129

magnesium oxide and superficial oxide layers on the silicon diatom frustules after the magnesiothermic conversion process. The decrease in elemental boron was also seen for samples prepared at original weight ratios of 0.5:1 and 2:1 of boric acid to silica (Table 1). There are 1.1- and 1.9-fold increases in boron concentration, respectively, for boron-doped silicon diatom frustules from 2:1 boric acid to silica weight ratios when compared to that for 1:1 and 0.5:1 samples, showing that it is possible to tune the boron doping.

Fabrication of a Diatom Photocathode and Photocurrent Density Measurements. Photoelectrodes were fabricated by hydrosilylation of boron-doped silicon diatom frustules with AM and subsequent immobilization of the frustules on a gold electrode surfaces' Au−S bonds. This procedure was followed from our previously published paper with slight modification (cf. Experimental Section for methodology).[25] An SEM micrograph (Figure 4, inset) displays the arrangement of AM hydrosilylated boron-doped silicon diatom frustules on a gold electrode used to establish photocurrent density measurements. The photocurrent density measurements were performed in two different electrolytes: phosphate buffer saline (PBS) and 0.1 M sulfuric acid (H_2SO_4). Figure 4 shows typical photocurrent density measurements of AM hydrosilylated boron-doped silicon diatom frustules (0.953 ± 0.054 ppm boron) fabricated on gold-coated glass electrodes. The bare AM hydrosilylated boron-doped silicon diatom frustules (bar I) showed a maximum photocurrent density (approximately −80 nA cm^{-2}). The negative shift in the photocurrent density measurements confirms the p-type semiconducting behavior of the bare AM hydrosilylated boron-doped silicon diatom frustules. The photocurrent density was found to be 1.6 times less than that of the AM hydrosilylated boron-doped silicon diatom frustules coated with InP NCs and catalyst (bar II) (approximately −130 nA cm^{-2}) at 0 V. At a bias potential of −500 mV (bar III), the AM hydrosilylated boron-doped silicon diatom frustules coated with InP NCs and catalyst showed a maximum photocurrent density of approximately −2 μA cm^{-2} (a 15-fold increase compared to that at 0 V). All of the above measurements were carried out in PBS electrolyte. When the measurement was carried out for the AM hydrosilylated boron-doped silicon diatom frustules coated with InP NCs and catalyst in 0.1 M H_2SO_4 at a bias potential of −500 mV (bar IV), we obtained an average photocurrent density of −4.8 μA cm^{-2} and maximum of approximately −6 μA cm^{-2}. Thus, acidic electrolytes improved the photocatalytic activity by accelerating the conduction and the donation of protons for reduction into H_2. Table 2 shows the corresponding OCP values of the electrodes.

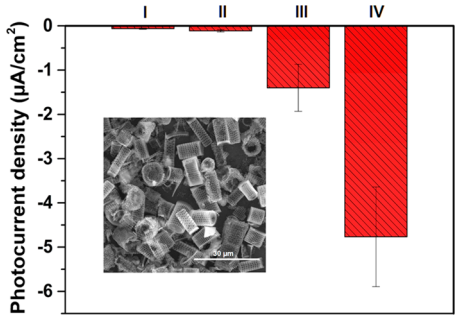

Figure 4. Photocurrent density measurements for bare AM hydrosilylated boron-doped silicon diatom frustules (0.953 ± 0.054 ppm boron) at 0 V (I), with InP NCs and catalyst at 0 V (II), and with InP NCs and catalyst at −500 mV (III) in PBS electrolyte. AM hydrosilylated boron-doped silicon diatom frustules with InP NCs and catalyst at −500 mV (IV) were measured in 0.1 M H_2SO_4 electrolyte. The inset shows the arrangement of boron-doped silicon diatom frustules on a gold electrode attached by means of AM hydrosilylation.

Figures S4A−C shows maximum current density measurements at bias potentials from 0 V to −500 mV in steps of 100 mV corresponding to the bar graph in Figure 4, bars I−IV, respectively. Prior to the deposition of InP and the catalyst, the OCP for bare boron-doped silicon diatom frustules in PBS electrolytes was −86 mV, compared to −143 mV after modification, which is 1.6 times higher. A positive shift in OCP of 34 mV was observed for boron-doped silicon diatom frustules modified with InP NCs and catalyst measured in 0.1 M H_2SO_4 electrolyte.

The current density measurements were conducted at −500 mV over 1.5 h to investigate the stability of AM hydrosilylated boron-doped silicon diatom frustules coated with InP NCs and catalyst in 0.1 M H_2SO_4 electrolyte (Figure 5). A bias potential of −500 mV resulted in an increase in the electrolytic activity, causing the current density trace to drop to −60 μA cm^{-2} (Figures 5 and S4C). We achieved a maximum photoelectric current density of −6 μA cm^{-2} for the AM hydrosilylated boron-doped silicon diatom frustules coated with InP NCs and catalyst (Figure S4C). The current density is shown to gradually decrease over time due to the oxidation of boron-doped silicon diatom frustules in the electrolyte solution (Figure 5).

Applied Bias Photo-to-Current Efficiency (ABPE) Calculation and H_2 Analysis. The ABPE was calculated using eq 1.[9,34] Table 3 shows the APBE efficiency calculated for

Table 2. OCPs and Electrolytes Used to Measure Photocurrent Densities Shown in Figure 4

trace	electrolytes	OCPs
I	PBS	−80.67 ± 5.03 mV
II	PBS	−120.66 ± 22 mV
III	PBS	−500 mV bias corresponding to −120.66 ± 22 mV OCPs
IV	0.1 M H_2SO_4	−500 mV bias corresponding to 9 ± 28.47 mV OCPs

DOI: 10.1021/acsami.5b04640
ACS Appl. Mater. Interfaces 2015, 7, 17381−17387

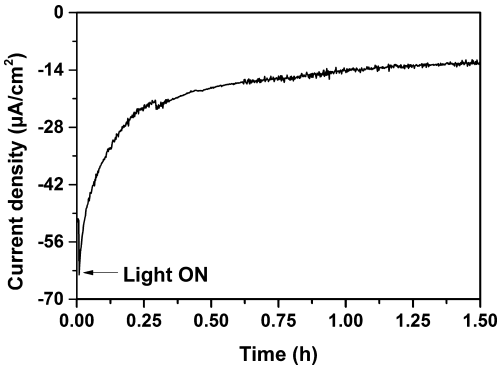

Figure 5. Current density measurements for 1.5 h carried out to determine the stability of the fabricated electrode in 0.1 M H_2SO_4 electrolyte.

Table 3. ABPE Efficiency Calculated for Photocurrent Densities Measured at Bias Potentials from −100 to −500 mV

bias potential	ABPE efficiency (%)
−100 mV	0.004
−200 mV	0.005
−300 mV	0.006
−400 mV	0.005
−500 mV	0.003

the bias potentials from −100 to −500 mV in steps of 100 mV in 0.1 M H_2SO_4 electrolyte. The maximum ABPE efficiency of 0.006% was observed at the −300 mV bias potential. Initially, bias potentials from −100 to −300 mV improved the efficiency. Further increasing the bias potentials to −400 and −500 mV decreased the efficiency to 0.005 and 0.003%, respectively. This is due to an increase in electrolytic activity as the photocatalytic activity decreased.

$$\text{ABPE} = \left[\frac{j\ (\text{mA cm}^{-2}) \times (1.23V - V_b)}{Pi\ (\text{mW cm}^{-2})}\right] \times 100\% \quad (1)$$

Here, j (mA cm^{-2}) is the measured photocurrent density; V_b is the bias among the working electrode, counter electrode, and reference electrode calculated vs NHE; and Pi is the incident light intensity (100 mW cm^{-2}).

For H_2 measurements, 310 μL of gas was collected after 1 h from the head space and injected into a GC. The peak value at 0.489 min (Figure 6) confirmed the presence of H_2.[35] The standard graph of H_2 (200 ppm) for 310 μL of a gas sample is shown in Figure S5. H_2 evolution was quantified to be 12.9 nmol using the area under the H_2 peaks from the GC measurements. Equations used to quantify H_2 evolution can be found in the Supporting Information. The theoretical amount of H_2 evolution for 6 μA cm^{-2} of photocurrent density for 1 h was calculated to be 112 nmol. This result indicates that 6 μA cm^{-2} of photocurrent density was not maintained for 1 h of measurement since the stability was not consistent, which is evident from Figure 5. Further tests to improve the stability of the fabricated electrodes for longer measurements using different passivation techniques are in progress. These photocurrent densities were somewhat smaller than those in our previously published results[9] on a synthetic porous silicon photocathode impregnated with InP NCs and $Fe_2S_2(CO)_6$ electrocatalyst. However, these photocurrents were 5.5 times

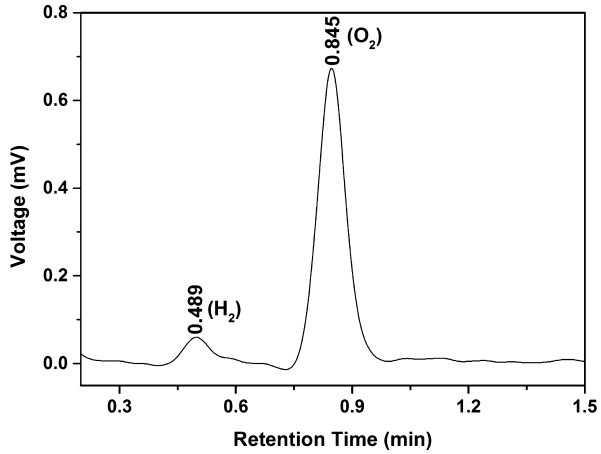

Figure 6. GC showing the presence of H_2 at a retention time of 0.489 min.

higher than those for magnesiothermically converted photoactive nanoporous silicon powder, which was fabricated with tin dioxide on fluorine doped tin oxide[36] in 0.1 M H_2SO_4 electrolyte under air mass 1.5 conditions. Our results demonstrate that a photocathode can be fabricated from naturally occurring diatom frustules.

CONCLUSIONS

Boron-doped silicon diatom frustules behaved as a p-type semiconducting material. Hydrosilylated doped diatom frustules in combination with InP NCs and $Fe_2S_2(CO)_6$ catalyst were able to produce a significant photocurrent density in comparison to that of bare doped silicon diatom frustules. We also report the first example of fabricating and sensitizing a p-type photocathode with diatom frustules to produce H_2. Our system gave a photocurrent density of approximately −6 μA cm^{-2} at a bias potential of −500 mV, and 12.9 nmol of H_2 for 1 h was produced for the boron doping concentration of about 0.953 ± 0.054 ppm. Photocurrent density measurements for different doping concentrations of elemental boron in silicon diatom frustules are underway. In addition, a tandem cell fabrication of n- and p-type silicon diatom frustules is also being carried out. We believe that harnessing naturally abundant diatoms could hold the key to cost-efficient renewable energy alternatives.

ASSOCIATED CONTENT

Supporting Information

Figure S1: SEM image showing the distorted shape of the boron-doped silicon diatom frustules after treatment with HCl and HF. Figure S2: XPS survey spectra of boron-doped silica diatom frustules and silicon diatom frustules. Figure S3: XRD spectrum of boron-doped silicon diatom frustules. Figure S4: Current density measurement for boron-doped silicon diatom frustules. Figure S5: GC of H_2 standard for 310 μL gas sample. Calculation for moles of H_2 produced. The Supporting Information is available free of charge on the ACS Publications website at DOI: 10.1021/acsami.5b04640.

AUTHOR INFORMATION

Corresponding Authors

*(T.N.) E-mail: thomas.nann@unisa.edu.au. Tel.: +61 8 830 25369. Fax: +61 8 830 23683.

DOI: 10.1021/acsami.5b04640
ACS Appl. Mater. Interfaces 2015, 7, 17381−17387

*(N.H.V.) E-mail: nico.voelcker@unisa.edu.au. Tel.: +61 8 8302 5508. Fax: +61 8 8302 5613.

Notes

The authors declare no competing financial interest.

■ ACKNOWLEDGMENTS

We would like to acknowledge Prof. Dusan Losic from University of Adelaide for providing diatom frustules. We would also like to thank Dr. Byuki Kawashima from University of South Australia for preparation of the samples for XANES analysis. This research was undertaken on the Soft X-ray Spectroscopy beamline at the Australian Synchrotron, Victoria, Australia.

■ REFERENCES

(1) Hisatomi, T.; Kubota, J.; Domen, K. Recent Advances in Semiconductors for Photocatalytic and Photoelectrochemical Water Splitting. *Chem. Soc. Rev.* **2014**, *43*, 7520−7535.
(2) Navarro, R. M.; del Valle, F.; Villoria de la Mano, J. A.; Álvarez-Galván, M. C.; Fierro, J. L. G. Photocatalytic Water Splitting under Visible Light: Concept and Catalysts Development. *Adv. Chem. Eng.* **2009**, *36*, 111−143.
(3) Navarro Yerga, R. M.; Álvarez Galván, M. C.; del Valle, F.; Villoria de la Mano, J. A.; Fierro, J. L. G. Water Splitting on Semiconductor Catalysts under Visible-Light Irradiation. *ChemSusChem* **2009**, *2*, 471−485.
(4) Currao, A. Photoelectrochemical Water Splitting. *Chimia* **2007**, *61*, 815−819.
(5) Sun, K.; Shen, S.; Liang, Y.; Burrows, P. E.; Mao, S. S.; Wang, D. Enabling Silicon for Solar-Fuel Production. *Chem. Rev.* **2014**, *114*, 8662−8719.
(6) Macdonald, T. J.; Mange, Y. J.; Dewi, M. R.; Islam, H. U.; Parkin, I. P.; Skinner, W. M.; Nann, T. CuInS2/ZnS Nanocrystals as Sensitisers for NiO Photocathodes. *J. Mater. Chem. A* **2015**, *3*, 13324−13331.
(7) Boettcher, S. W.; Warren, E. L.; Putnam, M. C.; Santori, E. A.; Turner-Evans, D.; Kelzenberg, M. D.; Walter, M. G.; McKone, J. R.; Brunschwig, B. S.; Atwater, H. A.; Lewis, N. S. Photoelectrochemical Hydrogen Evolution using Si Microwire Arrays. *J. Am. Chem. Soc.* **2011**, *133*, 1216−1219.
(8) Oh, I. W.; Kye, J.-H.; Hwang, S.-P. Fabrication of Metal-Semiconductor Interface in Porous Silicon and its Photoelectrochemical Hydrogen Production. *Bull. Korean Chem. Soc.* **2011**, *32*, 4392−4396.
(9) Chandrasekaran, S.; Macdonald, T. J.; Mange, Y. J.; Voelcker, N. H.; Nann, T. A Quantum Dot Sensitized Catalytic Porous Silicon Photocathode. *J. Mater. Chem. A* **2014**, *2*, 9478−9481.
(10) Macdonald, T. J.; Nann, T. Quantum Dot Sensitized Photoelectrodes. *Nanomaterials* **2011**, *1*, 79−88.
(11) Macdonald, T. J.; Mange, Y. J.; Dewi, M.; McFadden, A.; Skinner, W. M.; Nann, T. Cation Exchange of Aqueous CuInS2 Quantum Dots. *CrystEngComm* **2014**, *16*, 9455−9460.
(12) Jara, D. H.; Yoon, S. J.; Stamplecoskie, K. G.; Kamat, P. V. Size-Dependent Photovoltaic Performance of CuInS2 Quantum Dot-Sensitized Solar Cells. *Chem. Mater.* **2014**, *26*, 7221−7228.
(13) Kumar, B.; Beyler, M.; Kubiak, C. P.; Ott, S. Photoelectrochemical Hydrogen Generation by an [FeFe] Hydrogenase Active Site Mimic at a p-Type Silicon/Molecular Electrocatalyst Junction. *Chem. - Eur. J.* **2012**, *18*, 1295−1298.
(14) Tran, D. P.; Macdonald, T. J.; Wolfrum, B.; Stockmann, R.; Nann, T.; Offenhäusser, A.; Thierry, B. Photoresponsive Properties of Ultrathin Silicon Nanowires. *Appl. Phys. Lett.* **2014**, *105*, 231116.
(15) Sumper, M.; Brunner, E. Learning from Diatoms: Nature's Tools for the Production of Nanostructured Silica. *Adv. Funct. Mater.* **2006**, *16*, 17−26.
(16) Aw, M. S.; Simovic, S.; Yu, Y.; Addai-Mensah, J.; Losic, D. Porous Silica Microshells from Diatoms as Biocarrier for Drug Delivery Applications. *Powder Technol.* **2012**, *223*, 52−58.
(17) Jeffryes, C.; Gutu, T.; Jiao, J.; Rorrer, G. L. Metabolic Insertion of Nanostructured TiO2 into the Patterned Biosilica of the Diatom Pinnularia sp. by a Two-Stage Bioreactor Cultivation Process. *ACS Nano* **2008**, *2*, 2103−2112.
(18) Qin, T.; Gutu, T.; Jiao, J.; Chang, C. H.; Rorrer, G. L. Biological Fabrication of Photoluminescent Nanocomb Structures by Metabolic Incorporation of Germanium into the Biosilica of the Diatom Nitzschia frustulum. *ACS Nano* **2008**, *2*, 1296−1304.
(19) Yu, Y.; Addai-Mensah, J.; Losic, D. Synthesis of Self-Supporting Gold Microstructures with Three-Dimensional Morphologies by Direct Replication of Diatom Templates. *Langmuir* **2010**, *26*, 14068−14072.
(20) Losic, D.; Yu, Y.; Aw, M. S.; Simovic, S.; Thierry, B.; Addai-Mensah, J. Surface Functionalisation of Diatoms with Dopamine Modified Iron-Oxide Nanoparticles: Toward Magnetically Guided Drug Microcarriers with Biologically Derived Morphologies. *Chem. Commun.* **2010**, *46*, 6323−6325.
(21) Rosi, N. L.; Thaxton, C. S.; Mirkin, C. A. Control of Nanoparticle Assembly by using DNA-Modified Diatom Templates. *Angew. Chem.* **2004**, *116*, 5616−5619.
(22) Jantschke, A.; Herrmann, A. K.; Lesnyak, V.; Eychmüller, A.; Brunner, E. Decoration of Diatom Biosilica with Noble Metal and Semiconductor Nanoparticles (<10 nm): Assembly, Characterization, and Applications. *Chem. - Asian J.* **2012**, *7*, 85−90.
(23) Toster, J.; Iyer, K. S.; Xiang, W.; Rosei, F.; Spiccia, L.; Raston, C. L. Diatom Frustules as Light Traps Enhance DSSC Efficiency. *Nanoscale* **2013**, *5*, 873−876.
(24) Bao, Z.; Weatherspoon, M. R.; Shian, S.; Cai, Y.; Graham, P. D.; Allan, S. M.; Ahmad, G.; Dickerson, M. B.; Church, B. C.; Kang, Z.; Abernathy Iii, H. W.; Summers, C. J.; Liu, M.; Sandhage, K. H. Chemical Reduction of Three-Dimensional Silica Micro-Assemblies into Microporous Silicon Replicas. *Nature* **2007**, *446*, 172−175.
(25) Chandrasekaran, S.; Sweetman, M. J.; Kant, K.; Skinner, W.; Losic, D.; Nann, T.; Voelcker, N. H. Silicon Diatom Frustules as Nanostructured Photoelectrodes. *Chem. Commun.* **2014**, *50*, 10441−10444.
(26) Ge, M.; Rong, J.; Fang, X.; Zhang, A.; Lu, Y.; Zhou, C. Scalable Preparation of Porous Silicon Nanoparticles and their Application for Lithium-Ion Battery Anodes. *Nano Res.* **2013**, *6*, 174−181.
(27) Xu, S.; Ziegler, J.; Nann, T. Rapid Synthesis of Highly Luminescent InP and InP/ZnS Nanocrystals. *J. Mater. Chem.* **2008**, *18*, 2653−2656.
(28) Xu, S.; Kumar, S.; Nann, T. Rapid Synthesis of High-Quality InP Nanocrystals. *J. Am. Chem. Soc.* **2006**, *128*, 1054−1055.
(29) Ravel, á.; Newville, M. Athena, Artemis, Hephaestus: Data Analysis for X-ray Absorption Spectroscopy using IFEFFIT. *J. Synchrotron Radiat.* **2005**, *12*, 537−541.
(30) Bearden, J. A.; Burr, A. F. Reevaluation of X-Ray Atomic Energy Levels. *Rev. Mod. Phys.* **1967**, *39*, 125−142.
(31) Khouchaf, L.; Hamoudi, A.; Cordier, P. Evidence of Depolymerisation of Amorphous Silica at Medium- and Short-Range Order: XANES, NMR and CP-SEM Contributions. *J. Hazard. Mater.* **2009**, *168*, 1188−1191.
(32) Schreifels, J. A.; Maybury, P. C.; Swartz, W. E., Jr X-Ray Photoelectron Spectroscopy of Nickel Boride Catalysts: Correlation of Surface States with Reaction Products in the Hydrogenation of Acrylonitrile. *J. Catal.* **1980**, *65*, 195−206.
(33) Hendrickson, D. N.; Hollander, J. M.; Jolly, W. L. Core-Electron Binding Energies for Compounds of Boron, Carbon, and Chromium. *Inorg. Chem.* **1970**, *9*, 612−615.
(34) Ding, C.; Shi, J.; Wang, D.; Wang, Z.; Wang, N.; Liu, G.; Xiong, F.; Li, C. Visible Light Driven Overall Water Splitting using Cocatalyst/BiVO4 Photoanode with Minimized Bias. *Phys. Chem. Chem. Phys.* **2013**, *15*, 4589−4595.
(35) Zhang, K.; Jing, D.; Xing, C.; Guo, L. Significantly Improved Photocatalytic Hydrogen Production Activity over Photocatalysts

DOI: 10.1021/acsami.5b04640
ACS Appl. Mater. Interfaces 2015, 7, 17381−17387

Prepared by a Novel Thermal Sulfuration Method. *Int. J. Hydrogen Energy* **2007**, *32*, 4685−4691.
(36) Meekins, B. H.; Lin, Y.-C.; Manser, J. S.; Manukyan, K.; Mukasyan, A. S.; Kamat, P. V.; McGinn, P. J. Photoactive Porous Silicon Nanopowder. *ACS Appl. Mater. Interfaces* **2013**, *5*, 2943−2951.

DOI: 10.1021/acsami.5b04640
ACS Appl. Mater. Interfaces 2015, 7, 17381−17387